Materials Advances

ROYAL SOCIETY OF CHEMISTRY

PAPER

View Article Online
View Journal | View Issue



Cite this: *Mater. Adv.*, 2025, 6, 1191

# Synthetic route for high-yield α″-$Fe_{16}N_2$ submicron-sized powder using $CaH_2$ drying agent

Takayuki Tsuchida, *[a] Jun Fukushima,[a] Masahiro Tobise[b] and Hirotsugu Takizawa[a]

The rare-earth-free magnetic material α″-$Fe_{16}N_2$ is known to be a high-performance magnetic material. However, a synthetic route for high-yield α″-$Fe_{16}N_2$ powder has not yet been established. In this study, a high-yield α″-$Fe_{16}N_2$ submicron-sized powder was synthesized from $Fe_3O_4$ *via* $H_2$ reduction, and subsequent nitridation using a $CaH_2$ drying agent. Here, controlling the crystallite diameter of α-Fe is crucial to promoting nitridation. α-Fe powder with a crystallite diameter of approximately 20 nm was produced by lowering the reduction temperature and water vapor partial pressure. Thus, a high-yield α″-$Fe_{16}N_2$ phase of 97 wt% could be obtained. Microstructural observations indicated that α″-$Fe_{16}N_2$ submicron-sized powder with primary particles of 20–30 nm diameter could be synthesized. The α″-$Fe_{16}N_2$ powder had much higher coercivity than that of the α-Fe powder. Thus, the process suggested in this study is expected to contribute to the development of applications of α″-$Fe_{16}N_2$ in magnetic materials.

Received 23rd September 2024,
Accepted 30th December 2024

DOI: 10.1039/d4ma00961d

rsc.li/materials-advances



## 1. Introduction

Ferromagnetic materials have diverse applications, for example, in automotive motors and home appliances.[1,2] Two main ferromagnetic materials used for practical applications include Nd–Fe–B and Ferrite magnets. Of these, the former is known to be the strongest magnet in the world.[1–3] However, it is an expensive material, as it contains the rare-earth element Nd. The latter, *i.e.*, ferrite magnets are inexpensive, as they are rare-earth free; however, their magnetic performance is relatively low.[1,2] Thus, a rare-earth-free magnet with a magnetic performance exceeding that of ferrite is desired. α″-$Fe_{16}N_2$ meets the above-mentioned requirements and is expected to be a next-generation ferromagnetic material.[4]

Many studies related to α″-$Fe_{16}N_2$ have been reported on thin films[5–14] and nanoparticles,[4,15–29] ever since the giant magnetic moment of α″-$Fe_{16}N_2$ was discovered by Kim *et al.*[5] For instance, Sugita *et al.* fabricated single-crystal α″-$Fe_{16}N_2$ films by molecular beam epitaxy.[6] Ogawa *et al.* synthesized single-phase α″-$Fe_{16}N_2$ nanoparticles of approximately 100 nm by $H_2$ reduction and subsequent nitridation.[4] However, the synthesis of α″-$Fe_{16}N_2$ powder with a high bulk density is necessary for applications in ferromagnetic materials. Although there have been several reports on both powder[30–33] and bulk[34] forms of α″-$Fe_{16}N_2$, it contained some impurities, and its production yield was low, thus hindering its use in any practical applications. Therefore, it has become necessary to establish a synthetic route to high-yield α″-$Fe_{16}N_2$ powder for engineering applications.

Owing to the low diffusion rate of N atoms during $NH_3$ gas nitridation, powdering α″-$Fe_{16}N_2$ was a challenge that needed to be tackled. One previous study suggested that the smaller the crystallite size of α-Fe nanoparticles, the higher the yield of α″-$Fe_{16}N_2$ nanoparticles by nitridation.[15] Thus, we focused on controlling the crystallite diameter of α-Fe during $H_2$ reduction of iron oxide powder. In general, the nucleation and growth of nuclei during $H_2$ reduction depends on the reduction temperature and water vapor partial pressure;[35] therefore, the crystallite diameter of the α-Fe powder can be reduced by controlling these parameters. Our previous study demonstrated that the partial pressure of water vapor was lowered by introducing a drying agent, such as the $CaH_2$ into the $H_2$ reduction system, and the reduction reaction from the $Fe_3O_4$ powder to α-Fe powder was lowered from 400 to 300 °C.[36] Therefore, in this study, synthesis of high-yield α″-$Fe_{16}N_2$ submicron-sized powder was attempted *via* $H_2$ reduction and subsequent nitridation using a $CaH_2$ drying agent.

## 2. Materials and methods

A powder mixture sample (0.5 g) of $Fe_3O_4$ (Kojundo Chemical Lab. Co., 1 μm pass) and $CaH_2$ (Sigma–Aldrich Co., LCC) was weighed in a 20 : 80 weight ratio. The amount of $CaH_2$ is sufficient to absorb $H_2O$, which is produced by the reduction

[a] *Department of Applied Chemistry, Graduate School of Engineering, Tohoku University, Sendai 980-8579, Japan. E-mail: takayuki.tsuchida.r3@dc.tohoku.ac.jp*
[b] *Department of Electronic Engineering, Graduate School of Engineering, Tohoku University, Sendai 980-8579, Japan*

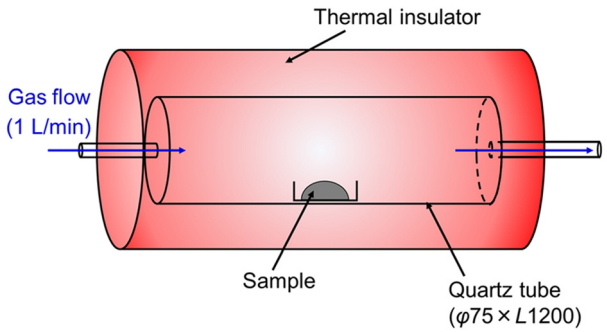


Fig. 1 Schematic diagram of the experimental setting.

reaction of $Fe_3O_4$. This is effective in lowering the partial pressure of water vapor within the system, thereby promoting the reduction reaction. Both mixed and unmixed samples were investigated. Each of these samples was placed in a tube furnace, as shown in Fig. 1. $H_2$ reduction was conducted at two temperatures, namely 300 or 400 °C for 4 h under a 1 L $min^{-1}$ $H_2$ gas flow. Subsequently, using an $N_2$ gas flow, the sample was cooled to ambient temperature. The sample was subsequently nitrided at a specific temperature in the range of 120–170 °C for 5 h under a 1 L $min^{-1}$ ammonia gas flow. After the nitridation, the sample was cooled to ambient temperature, using the $N_2$ gas flow. The sample was then slowly oxidized by increasing the oxygen partial pressure in stages to atmospheric concentration before being removed from the tube furnace. The obtained sample was washed several times with a 0.1 M $NH_4Cl$ (FUJIFILM Wako Pure Chemical Corporation) methanol solution and pure methanol to remove the by-products (CaO, $Ca(OH)_2$, and $CaH_2$), and subsequently dried in vacuum. Next, a phase analysis of the sample was conducted using X-ray diffraction (XRD) with Co-Kα source (Smart Lab, Rigaku); the microstructure of the samples was observed using transmission electron microscopy (TEM; EM-002B, TOPCON); and the magnetic properties of the samples were evaluated using superconducting quantum interference device (SQUID) measurements (MPMS, Quantum Design).

## 3. Results and discussion

### 3.1. Phase analysis of reduced samples

Fig. 2 shows the XRD profiles of the samples reduced under different conditions. The diffractions, under all the conditions, were assigned to α-Fe only, indicating that the reduction was complete as shown in chemical eqn (1). Table 1 shows the α-Fe crystallite diameter ($D_{Fe}$) values, calculated from the XRD profiles using Scherrer equation. First, the samples reduced at 400 °C with and without $CaH_2$ were compared. $D_{Fe}$ of the sample reduced with $CaH_2$ was smaller than that of the sample reduced without $CaH_2$. Next, the samples reduced with $CaH_2$ were compared. In this case, $D_{Fe}$ of the sample reduced at 300 °C was smaller than that of the sample reduced at 400 °C. From the above it was concluded that α-Fe with a smaller $D_{Fe}$ could be obtained using $CaH_2$ than with conventional $H_2$ reduction (*i.e.*, without a drying agent).

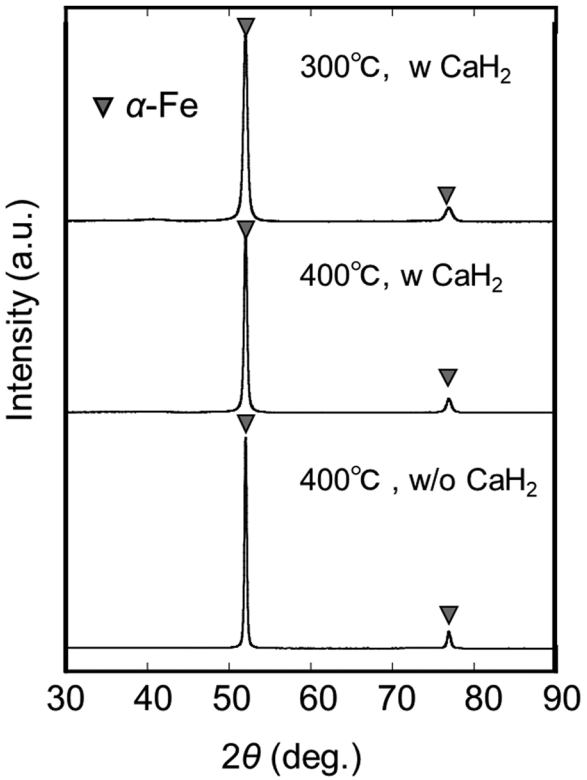


Fig. 2 XRD profiles of samples reduced under $H_2$ flow at two different temperatures with (w) and without (w/o) $CaH_2$.

Table 1 $D_{Fe}$ of samples reduced at two different temperatures with and without $CaH_2$

| | 400 °C w/o $CaH_2$ | 400 °C w $CaH_2$ | 300 °C w $CaH_2$ |
|---|---|---|---|
| $D_{Fe}$ (nm) | 41.8 | 27.8 | 19.5 |

$$Fe_3O_4 + 4H_2 \rightarrow 3\ (\alpha\text{-Fe}) + 4H_2O \quad (1)$$

Next, the effect of the $CaH_2$ drying agent and reduction temperature on $D_{Fe}$ will be discussed. For the samples reduced at 400 °C, $D_{Fe}$ decreased in the presence of $CaH_2$. Our previous study indicated that introducing the $CaH_2$ drying agent in the $H_2$ reduction system would lower the local partial pressure of water vapor in the iron oxide powder bed.[36] The decrease in the partial pressure of water vapor, accompanied by an increase in the partial pressure of $H_2$, would contribute to an increase in the reaction rate and promotion of nucleation of α-Fe. Therefore, it is understood that a decrease in $D_{Fe}$ in the presence of $CaH_2$ was owing to the promotion of α-Fe nucleation caused by a decrease in the partial pressure of water vapor. As regards the samples reduced with $CaH_2$, $D_{Fe}$ decreased upon lowering the reduction temperature from 400 to 300 °C. This might have been caused by the suppression of coarsening of the α-Fe crystallites. The mechanism described above is considered to be applicable to the reduction reactions of other oxides such as FeO and α-$Fe_2O_3$ as well. This will be explored in future work.

### 3.2. Phase analysis of nitrided samples

Fig. 3(a) shows the XRD patterns of the samples reduced at 400 °C for 4 h and subsequently nitrided at 160–170 °C for 5 h without $CaH_2$. Fig. 3(b) shows the production ratio of each phase calculated by reference intensity ratio (RIR) quantification. RIR quantification was performed using the software SmartLab Studio II (Rigaku), with PDF data for α″-$Fe_{16}N_2$ referenced from no. 654562, α-Fe from no. 191830, γ′-$Fe_4N$ from No. 79980, and ε-$Fe_3N$ from No. 93190. The samples nitrided at 170 °C contained the γ′-$Fe_4N$ phase, whereas those nitrided at 160 °C did not contain the γ′ phase. In addition, the samples nitrided at 170 °C contained more α-Fe phase than those nitrided at 160 °C. These results could be attributed to the decomposition of the α″-$Fe_{16}N_2$ phase into α-Fe and γ′-$Fe_4N$ phases.[37] Consequently, 78 wt% of the maximum yield of the α″-$Fe_{16}N_2$ phase was obtained from the nitridation of the samples reduced at 400 °C without $CaH_2$.

Fig. 4(a) shows the XRD patterns of the samples reduced at 400 °C for 4 h and subsequently nitrided at 120–170 °C for 5 h with $CaH_2$. Fig. 4(b) shows the production ratio of each phase as calculated by RIR quantification. The sample nitrided at 170 °C contained the γ′ phase, as well as the ε phase (which is an excessively nitrided phase), whereas that nitrided at 160 °C did not contain the ε phase. Additionally, the sample nitrided at 150–170 °C contained the γ′ phase, whereas that nitrided at 140 °C did not contain the γ′ phase, but contained α″ and α-Fe phases. The lower the nitridation temperature, the lower the yield of the α″ phase in 120–140 °C range. As a result, 77 wt% of the maximum yield of the α″-$Fe_{16}N_2$ phase was obtained from nitridation of the samples reduced at 400 °C with $CaH_2$.

Fig. 5(a) shows the XRD patterns of the samples reduced at 300 °C for 4 h, and subsequently nitrided at 130–170 °C for 5 h with $CaH_2$. Fig. 5(b) shows the production ratio of each phase, as calculated by RIR quantification. The sample nitrided at 160–170 °C contained γ′ and ε phases, whereas that nitrided at 150 °C did not contain any ε phase. Additionally, the sample nitrided at 150–160 °C contained the γ′ phase, whereas that nitrided at 140 °C did not contain the γ′ phase, but contained α″ and α-Fe phases. The lower the nitridation temperature, the lower the yield of the α″ phase in the range of 120–140 °C. As a result, 97wt% of the maximum yield of the α″-$Fe_{16}N_2$ phase was obtained from the nitridation of the samples reduced at 300 °C with $CaH_2$, which is more or less the α″ single phase.

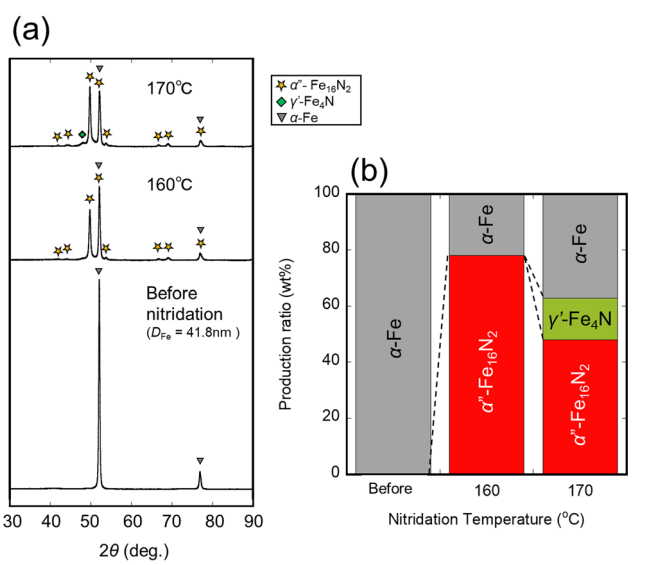


Fig. 3 (a) XRD profiles and (b) production ratio (wt%) of samples synthesized by $H_2$ reduction at 400 °C, and subsequently nitrided under $NH_3$ flow at different temperatures without $CaH_2$.

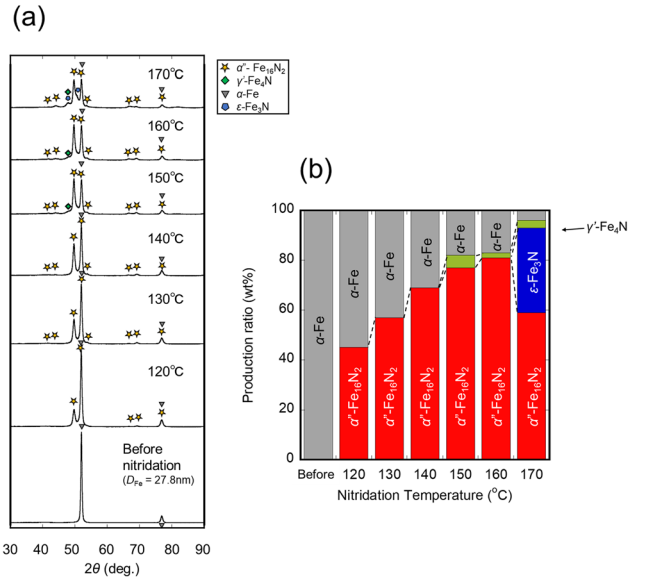


Fig. 4 (a) XRD profiles and (b) production ratio (wt%) of samples synthesize by $H_2$ reduction at 400 °C, and subsequently nitrided under $NH_3$ flow at different temperatures with $CaH_2$.

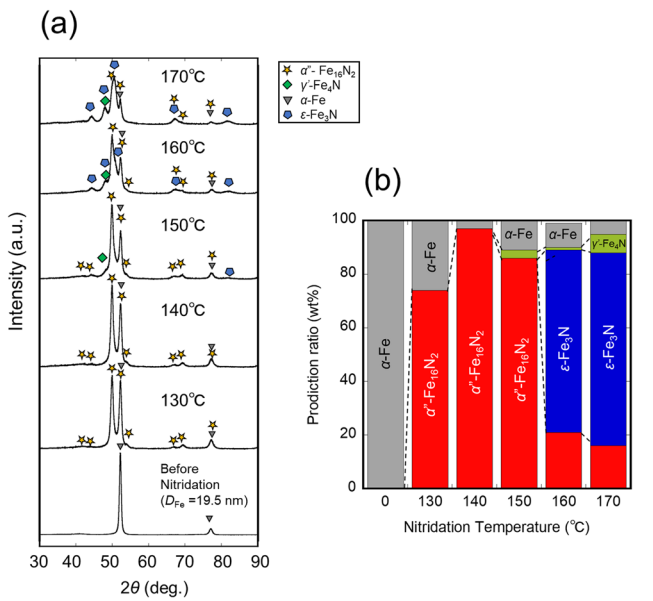


Fig. 5 (a) XRD profiles and (b) production ratio (wt%) of the samples synthesized by $H_2$ reduction at 300 °C, and subsequently nitrided under $NH_3$ flow at different temperatures with $CaH_2$.

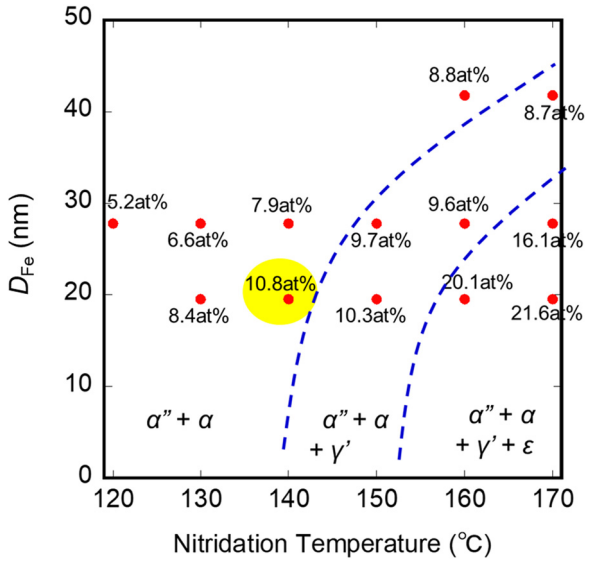


Fig. 6 Nitrogen content and formed phases as a function of nitridation temperature and $D_{Fe}$.

Fig. 6 shows a plot of the nitrogen content (at%) and the formed phase as a function of nitridation temperature and $D_{Fe}$, and reveals the effect of $D_{Fe}$ on the phase formation of iron nitrides. It was observed that the nitrogen content increased, and the nitridation temperature at which an excessively nitrided phase was obtained (as shown in chemical eqn (2) and (3)) was lowered with a smaller $D_{Fe}$. It was inferred that the activation increased with an increase in the crystallite interface, and the diffusion ability of nitrogen improved. As a result, a high-yield α″ phase was obtained by low-temperature nitridation (chemical eqn (4)), in which the decomposition of the α″ phase into α and γ′ (chemical eqn (5)) phases could be prevented.

$$6\ (\alpha\text{-Fe}) + 2NH_3 \rightarrow 2\ (\varepsilon\text{-}Fe_3N) + 3H_2 \quad (2)$$

$$8\ (\alpha\text{-Fe}) + 2NH_3 \rightarrow 2\ (\gamma'\text{-}Fe_4N) + 3H_2 \quad (3)$$

$$16\ (\alpha\text{-Fe}) + 2NH_3 \rightarrow \alpha''\text{-}Fe_{16}N_2 + 3H_2 \quad (4)$$

$$\alpha''\text{-}Fe_{16}N_2 \rightarrow 8\ (\alpha\text{-Fe}) + 2\ (\gamma'\text{-}Fe_4N) \quad (5)$$

### 3.3. Microstructure

Next, the microstructure of the reduced and nitrided samples was observed to understand the change in microstructure after $H_2$ reduction and subsequent nitridation. Fig. 7 shows the TEM images of the raw powder; sample reduced at 300 °C for 4 h with $CaH_2$; and subsequently nitrided at 140 °C for 5 h with $CaH_2$. The reduced sample was a submicron-sized powder with a nano-cluster structure comprising primary particles of 20–30 nm. The nitrided samples had almost the same structure. This result was consistent with the XRD measurements. Thus, submicron-sized α″-$Fe_{16}N_2$ powder with a nano-cluster structure consisting of primary particles of 20–30 nm was successfully synthesized *via* $H_2$ reduction and subsequent nitridation using the $CaH_2$ drying agent.

### 3.4. Magnetic properties

Two critical magnetic performance properties, namely coercivity ($H_c$) and saturation magnetization ($M_s$) of the α″-$Fe_{16}N_2$

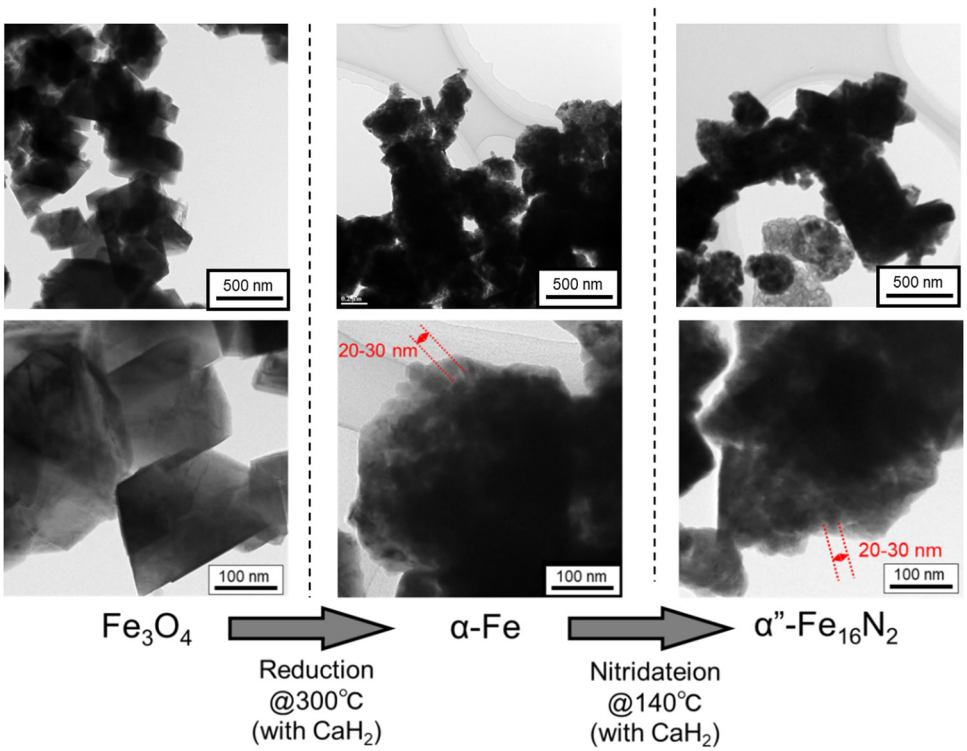


Fig. 7 TEM images of the raw material, reduced sample, and subsequently nitrided sample with $CaH_2$ drying agent.

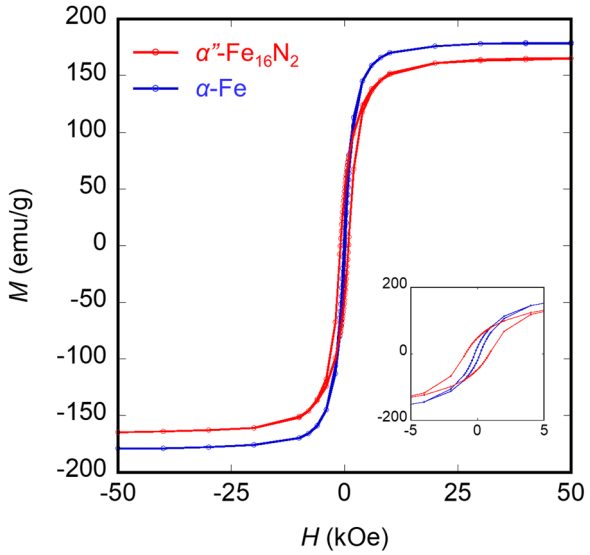


Fig. 8 $M$–$H$ curve of the sample reduced at 300 °C with $CaH_2$ drying agent (α-Fe, blue plot), and sample reduced at 300 °C with $CaH_2$ drying agent and subsequently nitrided at 140 °C (α″-$Fe_{16}N_2$, red plot) measured at 300 K.

powders produced were analyzed. Fig. 8 shows the room temperature $M$–$H$ curves of the sample reduced at 300 °C with $CaH_2$ (α-Fe powder), and sample reduced at 300 °C and nitrided at 140 °C with $CaH_2$ (α″-$Fe_{16}N_2$ powder). Table 2 lists $H_c$ and $M_s$ of each sample. $H_c$ of the α″-$Fe_{16}N_2$ powder was 892 Oe at 300 K which was higher than that of the α-Fe powder (203 Oe). Moreover, the ratio of coercivity at 300 K to 10 K shows a higher value for α″-$Fe_{16}N_2$ powder (∼0.95) than that for α-Fe powder (∼0.71). These suggest that the magnetic anisotropy $K_uV$ of α″-$Fe_{16}N_2$ is strong against thermal fluctuations $k_BT$, which is considered evidence of the high magnetic anisotropy of α″ phase. Additionally, $M_s$ of the α″-$Fe_{16}N_2$ powder was slightly smaller than that of the α-Fe powder. Thus, α″-$Fe_{16}N_2$ powder with high $H_c$ and $M_s$ could be synthesized *via* $H_2$ reduction and subsequent nitridation using the $CaH_2$ drying agent.

On the other hand, $M_s$ of the α-Fe and α″-$Fe_{16}N_2$ powders was much smaller than expected (222 emu $g^{-1}$ for the theoretical value of α-Fe and 234 emu $g^{-1}$ for nanoparticles of α″-$Fe_{16}N_2$).[4,38] In this study, the sample was slowly oxidized and exposed to air. Therefore, it was inferred that the small $M_s$ value was owing to the oxide film formed during the oxidization process. To further improve the magnetization, a process or an implementation that avoids oxidization is required.

Table 2 $H_c$ and $M_s$ of the sample reduced at 300 °C with $CaH_2$ drying agent (α-Fe), and sample reduced at 300 °C with $CaH_2$ drying agent and subsequently nitrided at 140 °C (α″-$Fe_{16}N_2$); $H_c$ and $M_s$ were measured at 10 K and 300 K

| | $H_c$ (Oe) | | $M_s$ (emu $g^{-1}$) | |
|---|---|---|---|---|
| | @10 K | @300 K | @10 K | @300 K |
| α″-$Fe_{16}N_2$ | 937 | 892 | 175 | 165 |
| α-Fe | 284 | 203 | 182 | 178 |

## 4. Conclusion

In this study, a high-yield α″-$Fe_{16}N_2$ submicron-sized powder, which is known to be a high-performance magnetic material, was synthesized *via* $H_2$ reduction and subsequent nitridation using $CaH_2$ as a drying agent. α-Fe powder with a small $D_{Fe}$ of 19.5 nm was produced *via* $H_2$ reduction at 300 °C for 4 h in the presence of $CaH_2$ drying agent. α″-$Fe_{16}N_2$ powder with a high yield of 97 wt% was successfully synthesized by nitridation of the α-Fe powder obtained as explained earlier at 140 °C for 5 h. From the microstructure observation, the α″-$Fe_{16}N_2$ powder had a nano-cluster structure consisting of primary particles of 20–30 nm diameter. Magnetic property measurements indicated that the synthesized α″-$Fe_{16}N_2$ powder had a high $H_c$ of 892 Oe and $M_s$ of 165 emu $g^{-1}$. The results of this study are significant for the application of α″-$Fe_{16}N_2$ as a magnetic material and contribute to the development of the automotive and home appliance industries. Experimental validation as a permanent magnet is necessary and will be addressed in future work.

## Data availability

All the data presented in this article are present in the form of figures and tables in the manuscript itself.

## Conflicts of interest

There are no conflicts to declare.

## Acknowledgements

This work was supported by the JSPS KAKENHI Grant-in-Aid for Scientific Research (S) Number JP19H05612. Magnetic measurements were performed at the Center for Low Temperature Science, Tohoku University. TEM measurements were performed at Institute for Materials Research, Tohoku University.

## References

1 R. W. McCallum, L. Lewis, R. Skomski, M. J. Kramer and I. E. Anderson, Practical Aspects of Modern and Future Permanent Magnets, *Annu. Rev. Mater. Res.*, 2014, **44**, 451–477, DOI: 10.1146/annurev-matsci-070813-113457.
2 S. Hirosawa, M. Nishino and S. Miyashita, Perspectives for High-Performance Permanent Magnets: Applications, Coercivity, and New Materials, *Adv. Nat. Sci: Nanosci. Nanotechnol.*, 2017, **8**, 013002, DOI: 10.1088/2043-6254/aa597c.
3 M. Sagawa, S. Fujimura, N. Togawa, H. Yamamoto and Y. Matsuura, New Material for Permanent Magnets on a Base of Nd and Fe (Invited, *J. Appl. Phys.*, 1984, **55**, 2083–2087, DOI: 10.1063/1.333572.

4 T. Ogawa, Y. Ogata, R. Gallage, N. Kobayashi, N. Hayashi, Y. Kusano, S. Yamamoto, K. Kohara, M. Doi, M. Takano and M. Takahashi, Challenge to the Synthesis of α″-$Fe_{16}N_2$ Compound Nanoparticle with High Saturation Magnetization for Rare Earth Free New Permanent Magnetic Material, *Appl. Phys. Express*, 2013, **6**, 14–17, DOI: 10.7567/APEX.6.073007.

5 T. K. Kim and M. Takahashi, New Magnetic Material Having Ultrahigh Magnetic Moment, *Appl. Phys. Lett.*, 1972, **20**, 492–494, DOI: 10.1063/1.1654030.

6 Y. Sugita, H. Takahashi, M. Komuro, K. Mitsuoka and A. Sakuma, Magnetic and Mössbauer Studies of Single-Crystal $Fe_{16}N_2$ and Fe–N Martensite Films Epitaxially Grown by Molecular Beam Epitaxy (Invited, *J. Appl. Phys.*, 1994, **76**, 6637–6641, DOI: 10.1063/1.358157.

7 Y. Sugita, H. Takahashi, M. Komuro, M. Igarashi, R. Imura and T. Kambe, Magnetic and Electrical Properties of Single-Phase, Single-Crystal $Fe_{16}N_2$ Films Epitaxially Grown by Molecular Beam Epitaxy (Invited, *J. Appl. Phys.*, 1998, **79**, 5576, DOI: 10.1063/1.362246.

8 P. Gupta, H. Fiedler, S. Rubanov and J. Kennedy, Magnetisation and Magnetic Anisotropy of Ion Beam Synthesised Iron Nitride, *J. Magn. Magn. Mater.*, 2021, **517**, 167388, DOI: 10.1016/j.jmmm.2020.167388.

9 J. P. Wang, N. Ji, X. Liu, Y. Xu, C. Sánchez-Hanke, Y. Wu, F. M. F. De Groot, L. F. Allard and E. Lara-Curzio, Fabrication of $Fe_{16}N_2$ Films by Sputtering Process and Experimental Investigation of Origin of Giant Saturation Magnetization in $Fe_{16}N_2$, *IEEE Trans. Magn.*, 2012, **48**, 1710–1717, DOI: 10.1109/TMAG.2011.2170156.

10 S. Higashikozono, K. Ito, F. Takata, T. Gushi, K. Toko and T. Suemasu, Highly Oriented Epitaxial (α″ + α′)-$Fe_{16}N_2$ Films on α-Fe(001) Buffered $MgAl_2O_4$(001) Substrates and Their Magnetization, *J. Cryst. Growth*, 2017, **468**, 691–695, DOI: 10.1016/j.jcrysgro.2016.11.048.

11 X. Hang, X. Zhang, B. Ma, V. Lauter and J. P. Wang, Epitaxial $Fe_{16}N_2$ Thin Film on Nonmagnetic Seed Layer, *Appl. Phys. Lett.*, 2018, **112**, 192402, DOI: 10.1063/1.5028396.

12 X. Zhang, Y. Jiang, M. Yang, L. F. Allard and J. P. Wang, High Ms $Fe_{16}N_2$ Thin Film with Ag under Layer on GaAs Substrate, *AIP Adv.*, 2016, **6**, 056203, DOI: 10.1063/1.4943236.

13 X. Zhang, V. Lauter, H. Ambaye and J. P. Wang, Thermal Stability of $Fe_{16}N_2$ Thin Film on GaAs (0 0 1) Substrate, *Mater. Res. Express*, 2017, **4**, 066401, DOI: 10.1088/2053-1591/aa72b3.

14 H. Y. Wang, E. Y. Jiang, H. L. Bai, Y. Wang, P. Wu and Y. G. Liu, The Effect of Ti Addition on the Thermal Stability of A″-$Fe_{16}N_2$, *J. Phys. D. Appl. Phys.*, 1997, **30**, 2932–2935, DOI: 10.1088/0022-3727/30/21/005.

15 M. Tobise, S. Saito and M. Doi, Challenge to the Synthesis of α″-(Fe, Co)$_{16}N_2$ Nanoparticles Obtained by Hydrogen Reduction and Subsequent Nitrogenation Starting from α-(Fe, Co)OOH, *AIP Adv.*, 2019, **9**, 035233, DOI: 10.1063/1.5079990.

16 J. Li, W. Yuan, X. Peng, Y. Yang, J. Xu, X. Wang, B. Hong, H. Jin, D. Jin and H. Ge, Synthesis of Fine α″-$Fe_{16}N_2$ Powders by Low-Temperature Nitridation of α-Fe from Magnetite Nanoparticles, *AIP Adv.*, 2016, **6**, 125104, DOI: 10.1063/1.4967950.

17 K. Suzuki, A. Towata, Y. Kinemuchi, D. Nagai and M. Yasuoka, Preparation of Highly Dispersed Core-Shell A″-$Fe_{16}N_2$/$SiO_2$ Particles Using Hydroxyapatite as a Sintering Prevention Layer, *J. Ceram. Soc. Jpn.*, 2017, **125**, 565–568, DOI: 10.2109/jcersj2.17037.

18 T. Ogi, Q. Li, S. Horie, A. Tameka, T. Iwaki and K. Okuyama, High-Purity Core-Shell A″-$Fe_{16}N_2$/$Al_2O_3$ Nanoparticles Synthesized from α-Hematite for Rare-Earth-Free Magnet Applications, *Adv. Powder Technol.*, 2016, **27**, 2520–2525, DOI: 10.1016/j.apt.2016.09.017.

19 P. Palade, C. Plapcianu, I. Mercioniu, C. Comanescu, G. Schinteie, A. Leca and R. Vidu, Structural, Magnetic, and Mössbauer Investigation of Ordered Iron Nitride with Martensitic Structure Obtained from Amorphous Hematite Synthesized via the Microwave Route, *Ind. Eng. Chem. Res.*, 2017, **56**, 2958–2966, DOI: 10.1021/acs.iecr.6b04574.

20 C. W. Kartikowati, A. Suhendi, R. Zulhijah, T. Ogi, T. Iwaki and K. Okuyama, Effect of Magnetic Field Strength on the Alignment of A″-$Fe_{16}N_2$ Nanoparticle Films, *Nanoscale*, 2016, **8**, 2648–2655, DOI: 10.1039/c5nr07859h.

21 M. Shibata, T. Ogawa and M. Kawashita, Synthesis of Iron Nitride Nanoparticles from Magnetite Nanoparticles of Different Sizes for Application to Magnetic Hyperthermia, *Ceram. Int.*, 2019, **45**, 23707–23714, DOI: 10.1016/j.ceramint.2019.08.086.

22 M. Tobise and S. Saito, Synthesis of α″-(Fe,M)$_{16}N_2$ Nanoparticles Obtained by Hydrogen Reduction and Subsequent Nitridation Starting from α-(Fe,M)OOH (M = Co, Al), *IEEE Trans. Magn.*, 2022, **58**, 2100505, DOI: 10.1109/TMAG.2021.3084603.

23 I. Dirba, M. Mohammadi, F. Rhein, Q. Gong, M. Yi, B. X. Xu, M. Krispin and O. Gutfleisch, Synthesis and Magnetic Properties of Bulk A″-$Fe_{16}N_2$/$SrAl_2Fe_{10}O_{19}$ Composite Magnets, *J. Magn. Magn. Mater.*, 2021, **518**, 167414, DOI: 10.1016/j.jmmm.2020.167414.

24 S. Kikkawa, A. Yamada, Y. Masubuchi and T. Takeda, Fine $Fe_{16}N_2$ Powder Prepared by Low-Temperature Nitridation, *Mater. Res. Bull.*, 2008, **43**, 3352–3357, DOI: 10.1016/j.materresbull.2008.02.008.

25 A. Suhendi, C. W. Kartikowati, R. Zulhijah, T. Ogi, T. Iwaki and K. Okuyama, Preparation and Characterization of Magnetic Films of Well-Dispersed Single Domain of Core-Shell α″-$Fe_{16}N_2$/$Al_2O_3$ Nanoparticles, *Adv. Powder Technol.*, 2015, **26**, 1618–1623, DOI: 10.1016/j.apt.2015.09.005.

26 J. Li, W. Yuan, X. Peng, Y. Yang, J. Xu, X. Wang, B. Hong, H. Jin, D. Jin and H. Ge, Synthesis of Fine α-$Fe_{16}N_2$ Powders by Low-Temperature Nitridation of α-Fe from Magnetite Nanoparticles, *AIP Adv.*, 2016, **6**, 125104, DOI: 10.1063/1.4967950.

27 S. Yamashita, Y. Masubuchi, Y. Nakazawa, T. Okayama, M. Tsuchiya and S. Kikkawa, Crystal Structure and Magnetic Properties of "α″-$Fe_{16}N_2$" Containing Residual α-Fe Prepared by Low-Temperature Ammonia Nitridation", *J. Solid*

*State Chem.*, 2012, **194**, 76–79, DOI: **10.1016/j.jssc.2012.07.025**.

28 I. Dirba, C. A. Schwöbel, L. V. B. Diop, M. Duerrschnabel, L. Molina-luna, K. Hofmann, P. Komissinskiy, H. Kleebe and O. Gutfleisch, Synthesis, Morphology, Thermal Stability and Magnetic Properties of $\alpha''$-$Fe_{16}N_2$ Nanoparticles Obtained by Hydrogen Reduction of $\gamma$-$Fe_2O_3$ and Subsequent Nitrogenation, *Acta Mater.*, 2017, **123**, 214–222, DOI: **10.1016/j.actamat.2016.10.061**.

29 Y. Matsumoto, Y. Masubuchi, Y. Nakazawa, H. Itami, M. Tsuchiya and S. Kikkawa, Core Loss in Magnetic Rings Made of $Fe_{16}N_2$-like Iron Nitride Powder, *J. Alloys Compd.*, 2019, **789**, 697–703, DOI: **10.1016/j.jallcom.2019.03.061**.

30 J. Kim, J. Hwang and S. Yi, Iron Nitride Based Magnetic Powder Synthesized by Mechanical Alloying of Fe-Based Glassy Powders and Solid Nitrogen Compounds, *J. Magn. Magn. Mater.*, 2021, **539**, 168329, DOI: **10.1016/j.jmmm.2021.168329**.

31 T. Saito, Production of Iron Nitrides by Mechanical Alloying, *J. Appl. Phys.*, 2000, **87**, 6514–6516, DOI: **10.1063/1.372755**.

32 I. Paseka, P. Bezdička, A. Kláriková and K. Závěta, Structure and Magnetic Properties of Ball-Milled Iron Nitride Powders, *J. Alloys Compd.*, 1998, **274**, 248–253, DOI: **10.1016/S0925-8388(98)00536-2**.

33 O. Zirhli, N. Gunduz Akdogan, Y. N. Odeh, I. B. Misirlioglu, E. Devlin and O. Akdogan, Fabrication and Characterization of $Fe_{16}N_2$ Micro-Flake Powders and Their Extrusion-Based 3D Printing into Permanent Magnet Form, *Adv. Eng. Mater.*, 2020, **22**, 2000311, DOI: **10.1002/adem.202000311**.

34 Y. Jiang, V. Dabade, L. F. Allard, E. Lara-Curzio, R. James and J. P. Wang, Synthesis of $\alpha''$-$Fe_{16}N_2$ Compound Anisotropic Magnet by the Strained-Wire Method, *Phys. Rev. Appl*, 2016, **6**, 024013, DOI: **10.1103/PhysRevApplied.6.024013**.

35 M. Elzohiery, H. Y. Sohn and Y. Mohassab, Kinetics of Hydrogen Reduction of Magnetite Concentrate Particles in Solid State Relevant to Flash Ironmaking, *Steel Res. Int.*, 2017, **88**(2), 1600133, DOI: **10.1002/srin.201600133**.

36 T. Tsuchida, J. Fukushima, M. Tobise, Y. Hayashi and H. Takizawa, Low-Temperature Hydrogen Reduction of Iron Oxide by Controlling the Water Potential Using a $CaH_2$ Drying Agent, *J. Solid State Chem.*, 2021, **302**, 122441, DOI: **10.1016/j.jssc.2021.122441**.

37 E. H. Du. Marchie van Voorthuysen, D. O. Boerma and N. C. Chechenin, Low-Temperature Extension of the Lehrer Diagram and the Iron-Nitrogen Phase Diagram, *Metall. Mater. Trans. A*, 2002, **33**, 2593–2598, DOI: **10.1007/s11661-002-0380-2**.

38 K. Song, C.-Y. Suh, K.-S. Ko, J.-H. Bang, W. Kim and I.-J. Shon, The Effect of Phases in Nanoparticles Produced by Electrical Wire Explosion on Arsenic(III) Removal, *Mater. Trans.*, 2012, **53**, 739–744, DOI: **10.2320/matertrans.M2011381**.